scientific reports

Check for updates

OPEN

A PCR amplicon-based SARS-CoV-2 replicon for antiviral evaluation

Tomohiro Kotaki[1]✉, Xuping Xie[2], Pei-Yong Shi[2] & Masanori Kameoka[1]✉

The development of specific antiviral compounds to SARS-CoV-2 is an urgent task. One of the obstacles for the antiviral development is the requirement of biocontainment because infectious SARS-CoV-2 must be handled in a biosafety level-3 laboratory. Replicon, a non-infectious self-replicative viral RNA, could be a safe and effective tool for antiviral evaluation. Herein, we generated a PCR-based SARS-CoV-2 replicon. Eight fragments covering the entire SARS-CoV-2 genome except S, E, and M genes were amplified with HiBiT-tag sequence by PCR. The amplicons were ligated and in vitro transcribed to RNA. The cells electroporated with the replicon RNA showed more than 3000 times higher luminescence than MOCK control cells at 24 h post-electroporation, indicating robust translation and RNA replication of the replicon. The replication was drastically inhibited by remdesivir, an RNA polymerase inhibitor for SARS-CoV-2. The IC_{50} of remdesivir in this study was 0.29 μM, generally consistent to the IC_{50} obtained using infectious SARS-CoV-2 in a previous study (0.77 μM). Taken together, this system could be applied to the safe and effective antiviral evaluation without using infectious SARS-CoV-2. Because this is a PCR-based and transient replicon system, further improvement including the establishment of stable cell line must be achieved.

Severe acute respiratory syndrome-coronavirus 2 (SARS-CoV-2) has been causing a catastrophic pandemic worldwide. The symptoms of SARS-CoV-2 infection (coronavirus disease 2019 [COVID-19]) ranges from asymptomatic to fever, acute respiratory distress, pneumonia, and ultimately death[1]. To date, several antiviral drugs such as remdesivir (viral RNA–dependent RNA polymerase [RdRp] inhibitor for Ebola virus) have been repurposed for COVID-19 therapy[2]. It is important to develop antiviral agents that can specifically inhibit the propagation of SARS-CoV-2. One of the obstacles for the antiviral evaluation of SARS-CoV-2 is biosafety concern. Because SARS-CoV-2 was classified as a biosafety level-3 (BSL-3) pathogen, it must be handled in a BSL-3 laboratory. The construction of a safe antiviral evaluation system has been coveted.

The replicon system could be a useful tool for safe and efficient antiviral evaluation. Replicon is a non-infectious, self-replicative RNA that lacks the viral structural genes and retains the genes necessary for RNA replication[3,4]. Because the replicon lacks viral structural genes, infectious virions are not produced from the transfected cell, thus reducing the biosafety concern. Additionally, the insertion of reporter gene into the replicon genome enables us to easily monitor the translation and replication of the replicon. The construction of a replicon system would accelerate the development of anti-SARS-CoV-2 agents.

SARS-CoV-2 belongs to the genus *betaoronavirus* of the family *coronaviridae*[5]. The genome of coronaviruses is single-stranded RNA ranging from 27 to 32 kb, the largest of any other known RNA viruses. Its large genome size and the existence of bacteriotoxic elements hindered the generation of reverse genetic systems and replicon. Several strategies have been adopted to overcome this obstacle: multiple plasmid system followed by in vitro DNA ligation or single bacterial artificial chromosome (BAC) plasmid system[6–8]. With these strategies, the infectious clones of SARS-CoV-2 and its reporter variants have been developed[9–13].

Herein, we generated a SARS-CoV-2 replicon by the in vitro ligation of PCR amplicons. The results demonstrated its use for antiviral evaluation without using the infectious SARS-CoV-2 virion.

Results

The construction of a SARS-CoV-2 replicon. We took an in vitro ligation strategy, similar to that used for constructing a SARS-CoV-2 infectious clone[9] (Fig. 1A,B). The genome of replicon included viral non-structural proteins (encoded in open reading frame [ORF]1a and 1b) and N protein that were required for RNA replication and discontinuous transcription of subgenomic RNAs. Meanwhile, the viral structural proteins (S, E, and M) were excluded so as not to produce infectious virion. Additionally, HiBiT-tag was incorporated into the C-terminus of N protein as an indirect readout for RNA replication and subgenomic RNA transcription of the

[1]Department of Public Health, Kobe University Graduate School of Health Sciences, 7-10-2 Tomogaoka, Suma-ku, Kobe, Hyogo 654-0142, Japan. [2]Department of Biochemistry and Molecular Biology, University of Texas Medical Branch, Galveston, TX, USA. ✉email: tkotaki@people.kobe-u.ac.jp; mkameoka@port.kobe-u.ac.jp

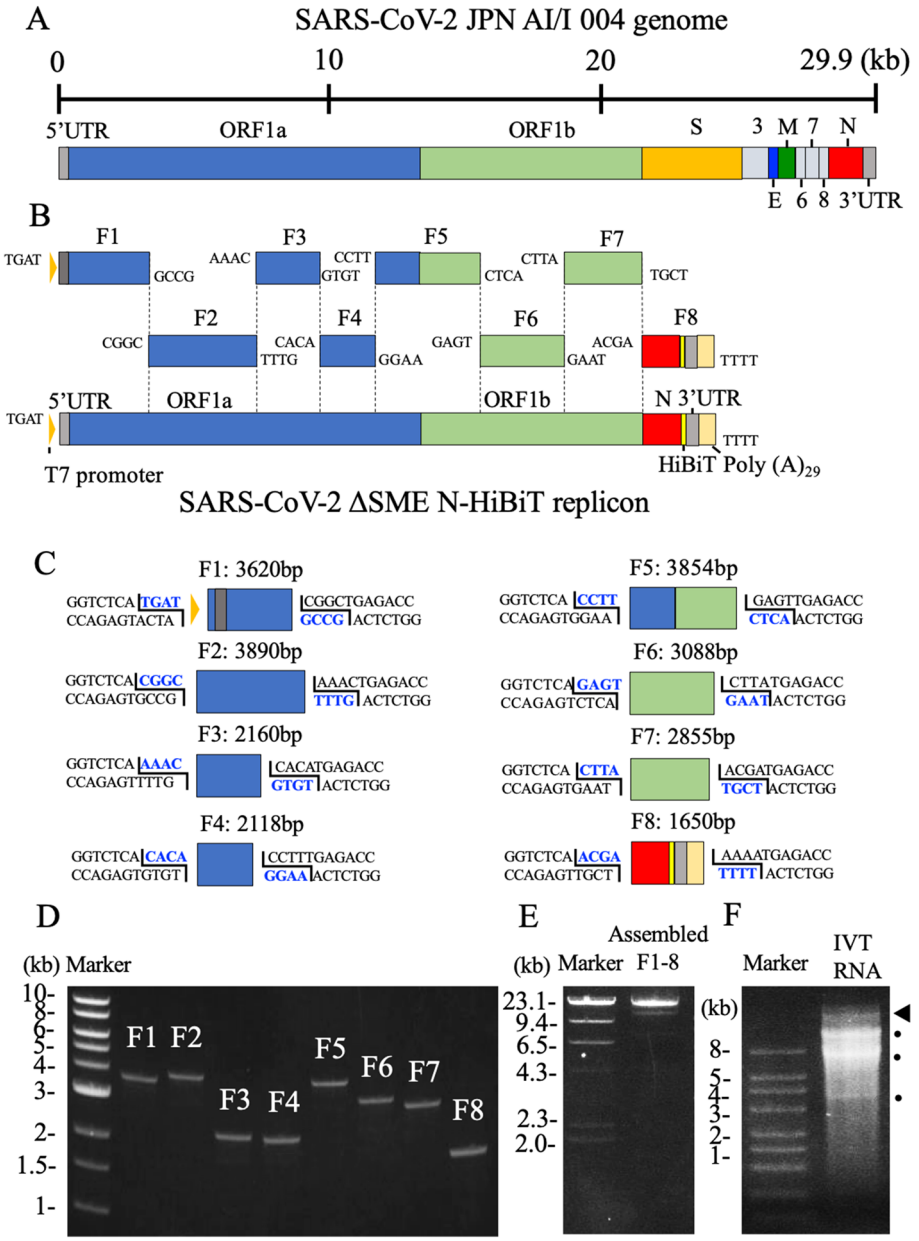

Figure 1. Construction of a SARS-CoV-2 replicon. (**A**) Genome structure of SARS-CoV-2. The untranslated regions (UTRs), open reading frames (ORFs), and structural proteins (S, E, M, and N) are indicated in this figure. (**B**) Strategy for the in vitro assembly of a SARS-CoV-2 replicon DNA. The nucleotide sequences of the overhang are indicated in this figure. The replicon DNA was assembled using in vitro ligation. (**C**) Detailed terminal sequences of each DNA fragment. Both 5′ and 3′ terminal sequences were recognized by BsaI. The overhang sequences were shown in blue. (**D**) Electrophoresis of the eight DNA fragments. Eight purified DNA fragments (about 100 ng) were run on a 1.0% agarose gel. The 1-kb DNA ladders are indicated in this figure. Original unedited gel image is shown in the supplementary dataset and image was not joined from different parts of the gel. (**E**) Electrophoresis of an assembled DNA. About 200 ng of assembled DNA was run on a 1% agarose gel. The λ-HindIII digest marker is indicated in this figure. Successfully assembled replicon DNA was 23.2 kb. Original unedited gel image is shown in the supplementary dataset and image was not joined from different parts of the gel. (**F**) Electrophoresis of RNA transcripts. About 1 μg of in vitro transcribed (IVT) RNAs were run under denaturing conditions. RNA ladders are indicated in this figure. The triangle indicates the genome-length RNA transcript (23 kb), whereas the circles show the shorter RNA transcripts. Because the biggest size of RNA marker was 8 kb, the estimation of the size of RNA transcripts was not accurate. Original unedited gel image is shown in the supplementary dataset and image was not joined from different parts of the gel.

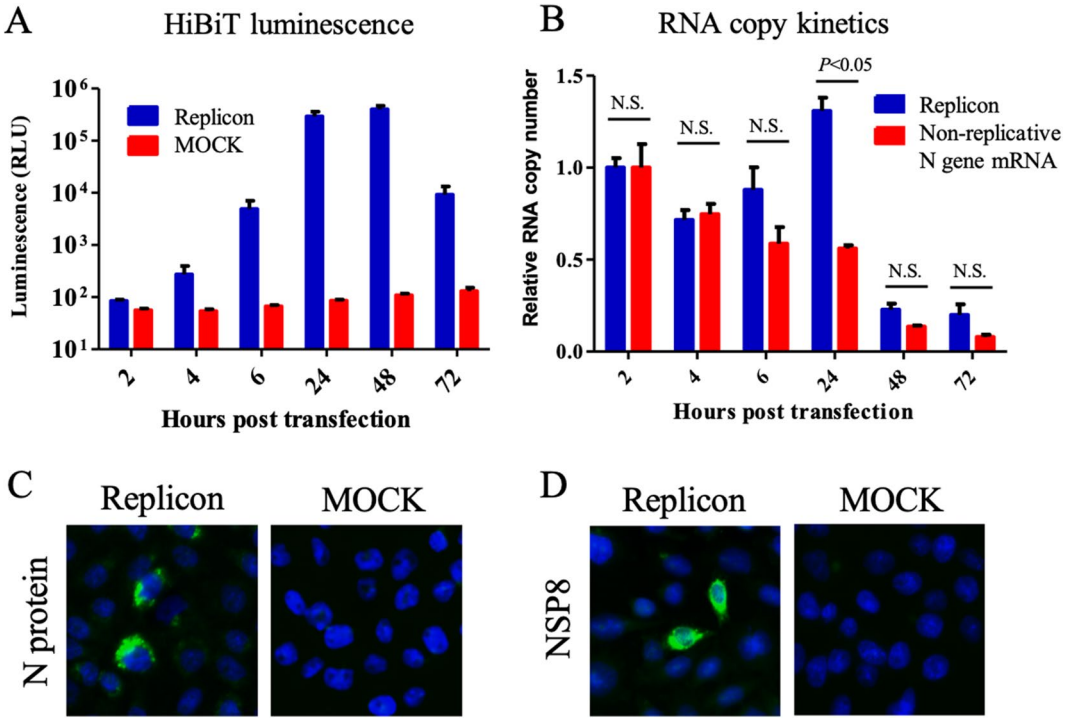

Figure 2. Characterization of a SARS-CoV-2 replicon. (**A**) Kinetics of luminescence signal. The CHO-K1 cells were electroporated with 5 μg of replicon RNA. Intracellular luminescence signals were measured at the indicated time points. The mean and standard error of two independent experiments are shown in this figure. (**B**) Kinetics of the RNA copy. The CHO-K1 cells were electroporated with 10 μg of either the replicon RNA or the non-replicative N gene mRNA. RNA copy numbers were subsequently measured using qRT-PCR. The results were expressed as relative RNA copy number compared to that at 2 hpt. Multiple t-tests were performed for determining the statistical significance. A p-value < 0.05 was considered to be statistically significant. *NS* not significant. (**C**) The detection of N protein by IFA. The CHO-K1 cell was electroporated with 5 μg of replicon RNA. The cells were fixed with 4% paraformaldehyde, followed by permeabilization with 0.5% Triton-X. The expression of N protein was detected using anti-N mAb and goat-anti-mouse IgG conjugated with Alexa Fluor 488. Nucleus was stained by DAPI. (**D**) The detection of NSP8 protein by IFA. The expression of NSP8 protein was detected using anti-NSP8 mAb and goat-anti-mouse IgG conjugated with Alexa Fluor 488.

transfected replicon. SARS-CoV-2 5′ untranslated region (UTR), ORF1a, and 1b were separately amplified in the fragment 1 (F1) to F7. Then, N (including the closest transcription regulatory sequence [TRS] on 5′ upstream: ACGAACAAACTAAA), HiBiT-tag, and 3′UTR were amplified in the F8. Each amplicon comprised the BsaI recognition sites at the both 5′ and 3′ termini. Figure 1C shows the detailed information of the fragments.

The viral RNA extracted from the culture fluid of SARS-CoV-2–infected Vero E6 cell was used as a template for RT-PCR. Table S1 shows the primer sets used for the amplification of above-described eight fragments (Fig. 1D). The fragments were assembled in a two-step ligation: (1) all the eight fragments were digested with BsaI, followed by the ligation of two adjacent fragments (e.g. F1 and F2 for F1–2) to produce four assembled fragments; (2) the ligated fragments were gel extracted and mixed, followed by a further ligation to construct the full-length replicon DNA. The size of the successfully ligated replicon DNA was 23.2 kb (Fig. 1E). In vitro transcription using the replicon DNA produced multiple bands (Fig. 1F). Of these bands, the highest band might represent the full-size replicon (indicated by arrow). Because the biggest size of RNA marker was only 8 kb, the estimation of the size of RNA transcripts was not accurate.

Characterization of a SARS-CoV-2 replicon. The in vitro transcribed RNA was directly electroporated (without gel purification) into CHO-K1, BHK-21, or HEK-293T cells to determine the most robust replicon system. In the CHO-K1 cell, the HiBiT signals started to increase as early as 4–6 h post-transfection (hpt), indicating translation and replication of the replicon (Fig. 2A). At 24–48 hpt, the signals increased by more than 3000 times than the MOCK control. However, the signals decreased at 72 hpt, indicating degradation of the N-HiBiT protein. The BHK-21 and HEK-293T cells showed less HiBiT signals over time (Figure S1). Thus, the CHO-K1 cell was the most suitable cell line for the robust replication of the replicon, and used for the subsequent experiments.

Subsequently, the kinetics of the replicon RNA in the transfected cells were examined using quantitative reverse transcription PCR (qRT-PCR). The mRNA encoding N gene was also electroporated as a non-replicative RNA control[9]. A decrease was observed for both RNAs at 4 hpt, indicating RNA degradation (Fig. 2B). At 6–24 hpt, the quantity of replicon RNA started to increase, whereas that of the non-replicative RNA showed a

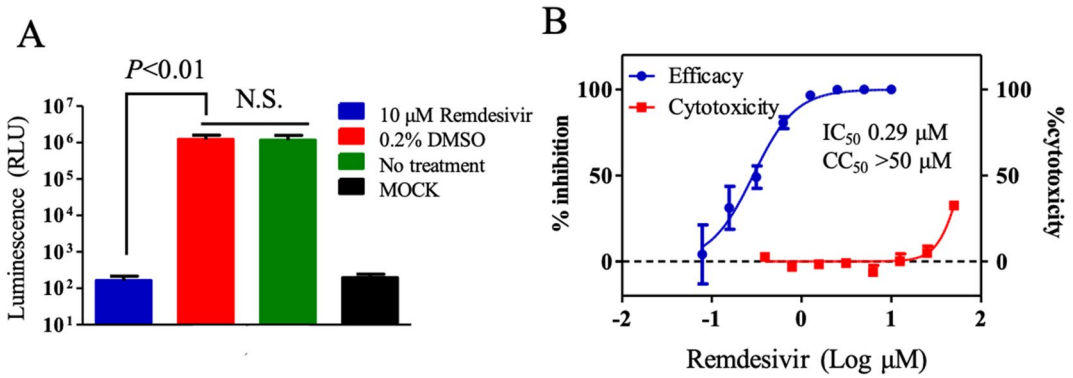

Figure 3. Antiviral evaluation using SARS-CoV-2 replicon. (**A**) Antiviral activity of remdesivir. The CHO-K1 cells electroporated with 5 μg of replicon RNA were seeded in a 96-well plate. The cells were treated immediately with 10-μM remdesivir or 0.2% DMSO. Luminescence was measured at 24 h post-treatment. The mean and standard error of two independent experiments are shown in this figure. A one-way ANOVA was performed to determine the statistical significance. A *p*-value less than 0.05 was considerd to be statistically significant. *NS* not significant. (**B**) Calculation of IC_{50} and CC_{50}. The CHO-K1 cells electroporated with replicon RNA was seeded. The cells were immediately treated with remdesivir at indicated concentrations. Luminescence and cell viability were measured at 24 h post-treatment. IC_{50} and CC_{50} values were calculated by GraphPad software. The mean and standard error of two independent experiments are shown in this figure.

continuous decrease, indicating replication of the replicon. At 48–72 hpt, both the RNAs had been decreased drastically. To investigate the cause of replicon RNA destabilization, the mRNA levels of interferon-β (IFN-β) and Mx1 in the transfected cells were examined. The expression of IFN-β and Mx1 genes was upregulated in the cells (Figure S2), indicating the induction of interferon signaling in replicon-transfected cells.

The viral N protein and NSP8 (a component of RNA replication complex encoded in ORF1a) expressions were confirmed by immunofluorescence assay (IFA) (Figs. 2C,D, S3). The NSP8 protein localized not only to the reticular pattern but also to dots (Figure S3)[14,15]. The ratio of viral protein positive cell was less than 1%. These data indicated that the replicon was successfully constructed and replicative.

Antiviral evaluation. Next, we tested if this RNA replicon could be used for antiviral evaluation. Remdesivir, an RdRp inhibitor effective for SARS-CoV-2, was used as a control compound. In total, 10 μM of remdesivir significantly inhibited the translation and replication of the replicon, whereas dimethyl sulfoxide (DMSO) control did not (Fig. 3A). The 50% inhibitory concentration (IC_{50}) and 50% cytotoxicity concentration (CC_{50}) values were calculated to 0.29 μM and more than 50 μM, respectively (selectivity index [SI] > 172.4) (Fig. 3B). The IC_{50} value estimated using our replicon system was about 2.6 times lower than the previously reported IC_{50} (0.77 μM)[16]. A previous study infected Vero E6 with infectious SARS-CoV-2 in the presence of remdesivir, and quantified the virus released in the supernatant by qRT-PCR at 48 h post-infection[16]. The differences of our replicon assay and previous infectious SARS-CoV-2 assay including cell line (CHO or Vero), incubation time (24 h or 48 h), and action point of analysis (only translation and RNA replication or whole viral replication steps) might cause the difference in IC_{50}. Indeed, the difference of the cell line caused different IC_{50} values of remdesivir[17]. Nevertheless, the result was generally consistent with the previous report, thus demonstrating that our replicon system could be used for antiviral evaluation.

Discussion

SARS-CoV-2 is an emergent threat worldwide. A high throughput and safe antiviral evaluation system is urgently needed to identify the anti-SARS-CoV-2 compound, which has not yet been developed. Several plasmid-based SARS-CoV-2 replicons have been reported[18,19]. Here, we reported a SARS-CoV-2 replicon system with PCR amplicon-based strategy. The advantage of this system is its technical simplicity. Additionally, this system enabled us to produce a replicon without generating genetically modified *E. coli*. Thus, bacteriotoxic elements in the SARS-CoV-2 genome do not affect the construction of the replicon. However, the PCR-based strategy might be inferior to the plasmid-based strategy in terms of the yield of replicon RNA and usability of genome modification. Additionally, PCR-based replicon might contain the undesired mutations, which are undetectable by Sanger sequence. Nevertheless, this PCR-based replicon system offered an alternative way over plasmid-based replicon, especially in the resource-limited settings.

The cells electroporated with the replicon RNA showed more than 3,000 times higher luminescence as compared to the MOCK control cells at 24 hpt (Fig. 2A). However, the replicon RNA copy was increased by only 1.5 times at 24 hpt compared to that at 2 hpt (Fig. 2B); this could be attributed to RNA degradation and low positive rate of successful replication of the replicon in the cells (< 1%). Nevertheless, the replicon showed a significant increase in the RNA copy compared to the non-replicative control RNA at 24 hpt, indicating RNA replication. The replicon RNA copy as well as the HiBiT signal started decreasing at 48 hpt and 72 hpt, respectively, indicating low stability of the replicon. This discrepancy was considered due to the higher stability of N-HiBiT protein

than that of the replicon RNA. The mRNA levels of IFN-β and Mx1 were increased in replicon-transfected cells (Figure S2), suggesting the role of interferon signaling on the rapid decrease of replicon RNA. Further studies such as testing the replicon transfection in CHO-K1 cells upon inhibition of IFN-β production and/or Jak-STAT signaling are needed to validate this notion.

In this study, CHO-K1, BHK-21, and 293T cells were used because these cell lines were used for the construction of coronavirus replicon and coronavirus protein expression[3,4]. However, only CHO-K1 supported the robust replication of the replicon. Interestingly, even BHK-21, which is defective of IFN production, showed less replication of the replicon[20]. This was not attributed to the electroporation efficacy because the difference of input RNA in each cell was observed to exhibit an enhancement within twofold (Figure S4A). CHO-K1 showed the highest fold enhancement of the replicon copy number at 24 hpt among the three cell lines (Figure S4B). The obtained data suggested that the host factors other than IFN might be related to the lower replication of SARS-CoV-2 replicon in BHK-21 and 293T cells, although further analysis is needed.

We chose to fuse HiBiT-tag to the N protein because subgenomic mRNA-encoding N was the most abundantly produced mRNA during the replication of coronavirus[21]. This study demonstrated that the insertion of HiBiT-tag at the C-terminus of N protein did not disrupt the RNA replication. This finding could be applied to the construction of HiBiT-tagged reporter infectious virus[22]. We had also tried to fuse HiBiT-tag at the N-terminus of N protein (Figure S5A, S5B, and Table S2). The luminescence of the replicon with N-terminal HiBiT was 10 times lower than that with C-terminal HiBiT at 24 hpt (Figure S5C). The N protein is involved in not only nucleocapsid formation, but also RNA replication such as helicase activity and genome-length negative-strand RNA synthesis[23,24]. Although the N-terminus of N protein was not associated with either RNA binding or dimerization[25], the modification of the N-terminus might affect the replication efficacy. Alternatively, the position of HiBiT-tag in the N protein might have affected the sensitivity of HiBiT assay.

This replicon system can be used not only for antiviral evaluation but also for the analysis of SARS-CoV-2 ORF1ab function in terms of RNA replication. SARS-CoV-1 replicon was applied to the functional analysis of non-structural proteins encoded in ORF1[4]. Nowadays, several mutations have been observed in the replication complex regions because of worldwide pandemic[26]. For example, the virological meaning of ORF1ab 4715L mutation positively correlated to a high fatality rate remains unknown[27]. This system would help to shed light on the enigmatic SARS-CoV-2 RNA replication mechanism.

The disadvantages of this system were that our replicon was a transient expression system, which was not a high throughput system. The cell line stably carrying the replicon gene needs to be established by inserting the antibiotic resistance gene such as puromycin N-acetyl-transferase into the replicon genome[3]. Additionally, our replicon lacks the structural genes including S, E, and M. Thus, this system cannot be used for the compounds acting on receptor binding, virus entry, encapsidation, and virus release. These targets could be covered by using a single-round infectious pseudo-type reporter virus usable in the BSL-2 laboratory[28].

In conclusion, we reported a SARS-CoV-2 replicon that can be applied to antiviral evaluation without using infectious virion. Further improvement of this replicon system would accelerate the antiviral screening and help to identify the novel drug candidates for COVID-19.

Materials and methods

Virus and cell line. A clinical SARS-CoV-2 isolate from Japan (JPN AI-I 004 strain; EPI_ISL_407084) was used for the construction of replicon. Baby hamster kidney-21 (BHK-21) cell (ATCC: CCL-10) was maintained in the Eagle's minimal essential medium (MEM) supplemented with 10% fetal bovine serum (FBS) at 37 °C with 5% CO_2. Chinese hamster ovary-K1 (CHO-K1) cell (ATCC: CCL-61) was maintained in MEM supplemented with 10% FBS, non-essential amino acids at 37 °C with 5% CO_2. HEK-293 T cell (ATCC: CRL-3216) was maintained in the DMEM supplemented with 10% FBS.

The construction of a SARS-CoV-2 replicon DNA. The viral RNA extracted from the culture fluid of SARS-CoV-2–infected Vero E6 cell (provided by the National Institute of Infectious Diseases, Japan) was reverse transcribed into cDNA by the SuperScript III First Strand Synthesis system (Thermo Fisher Scientific) with random hexamer primers. The fragments were amplified by primer sets (Table S1) and high-fidelity PCR with the Platinum SuperFi II DNA polymerase (Thermo Fisher Scientific). F8 was generated by the overlap PCR of F8A and F8B fragments to insert the HiBiT-tag at the C-terminus of N gene (Table S1). The overhang sequences after BsaI digestion were designed based on the ligase fidelity viewer program (available at the New England Biolabs website).

For assembly, all the fragments were digested with BsaI-HF v2 (New England Biolabs) and purified directly using NucleoSpin Gel and PCR clean-up (Macherey–Nagel). Then, two adjacent fragments of equimolar amount were mixed and ligated with 400 units of T4 DNA ligase (New England Biolabs) at 4 °C overnight: F1 (1.45 μg) and F2 (1.56 μg) for F1–2, F3 (0.86 μg) and F4 (0.85 μg) for F3–4, F5 (1.54 μg) and F6 (1.24 μg) for F5–6, and F7 (1.14 μg) and F8 (0.66 μg) for F7–8. The assembled fragments were electrophoresed on a 1% agarose gel and extracted using Monofas DNA extraction kit (GL Science). Then, extracted fragments were mixed and further assembled with 2,000 units of T4 DNA ligase at 4 °C overnight. The assembled DNA was directly purified by phenol–chloroform–isoamyl alcohol (25:24:1), by chloroform, and isopropanol precipitate. The pelleted DNA was washed once with 70% ethanol, dried by air, and finally dissolved in 10 μl of DEPC-treated water.

RNA transcription, electroporation, and luminescence quantification. The replicon RNA was transcribed by the mMESSAGE mMACHINE T7 Transcription Kit (Thermo Fisher Scientific) according to the manufacturer's instruction with some modifications. Cap analog to GTP ratio was set to 1:1. About 1 μg of the assembled DNA was subjected to RNA transcription. The reaction was incubated at 30 °C overnight. Addition-

ally, a SARS-CoV-2N gene mRNA was in vitro transcribed following a report[9]. After removing the DNA template following the manufacturer's protocol, RNA was extracted by phenol–chloroform and isopropanol precipitated. The pelleted RNA was washed once with 70% ethanol, dried by air, and dissolved in 40 µl of DEPC-treated water. The RNA was electrophoresed using DynaMarker RNA High for Easy Electrophoresis (BioDynamics Laboratory. Inc.) for the rough quality check.

The RNA was electroporated using NEPA21 electroporator (Nepagene). The cells were trypsinized and washed twice with Opti-MEM (Thermo Fisher Scientific). The washed cells (1×10^6 cells) were mixed with 5 µg of replicon RNA in 100 µL of Opti-MEM. Electric pulses were given by NEPA21. The parameters for BHK-21 and CHO-K1 cells were as follows: voltage = 145 V; pulse length = 5 ms; pulse interval = 50 ms; number of pulses = 1; decay rate = 10%; polarity + as poring pulse and voltage = 20 V; pulse length = 50 ms; pulse interval = 50 ms; number of pulses = 5; decay rate = 40%; and polarity + / − as transfer pulse. The parameters for 293 T cell was same as above except voltage 150 V and pulse length of 2.5 ms for poring pulse. After electroporation, the cells were seeded as 1.5×10^4 cells/well in a 96-well plate. At various time points post-transfection, the cells were lysed with 25 µl of Nano-Glo HiBiT lytic detection system (Promega) plus 25 µl of PBS. The luminescence signal was detected by CentroPRO LB962 (Berthold Technologies).

Quantitative reverse transcription PCR (qRT-PCR). Cells electroporated with 10 µg of the replicon RNA or N gene mRNA were seeded at a concentration of 1.0×10^5 cells/well in a 24-well plate. Total intracellular RNAs were subsequently extracted from the transfected cells using an RNeasy minikit (Qiagen). Extracted RNAs were then eluted in 50 µl of RNase-free water. The RNA copy number was measured using a QuantiTect Probe RT-PCR Kit (Qiagen). CDC-approved primers (CDC_2019-nCoV_N2-F and CDC_2019-nCoV_N2-R) and a probe (CDC_2019-nCoV_N2-P) targeting the SARS-CoV-2N gene were used[29]. The probe contained a 6-carboxyfluorescein (FAM) reporter dye at the 5′-end and a Black Hole Quencher (BHQ) at the 3′-end. An in vitro transcribed SARS-CoV-2N gene was used as the RNA standard for the qRT-PCR. The mRNA levels of IFN-β, Mx1, and the housekeeping gene encoding glyceraldehyde-3-phophate dehydrogenase (GAPDH) were measured using an iScript one-step RT-PCR kit with SYBR green (Bio-Rad). The probe and primers used for qRT-PCR were listed in Table S3. Subsequently, 20 µl reaction mixtures were set up with 2 µl of RNA for all qRT-PCRs. All the assays were conducted using CFX Connect Real-Time PCR System (Bio-Rad).

Immunofluorescence assay. At 24 hpt, the cells were fixed with 4% paraformaldehyde, followed by permeabilization with 0.5% Triton-X. After blocking with normal goat serum, the cells were incubated with primary mouse monoclonal antibodies (mAbs) (anti-N mAb [6H3: GeneTex] or anti-NSP8 mAb [5A10: GeneTex]) followed by a secondary antibody (goat anti-mouse IgG conjugated with Alexa Fluor 488). The cells were mounted in a mounting medium containing 4′,6-diamidino-2-phenylindole (DAPI: Vector Laboratories). Fluorescence images were acquired by a fluorescence microscope. Blue- and green-fluorescence images were merged in ImageJ software[30].

Antiviral treatment. The CHO-K1 cells electroporated with 5 µg of the replicon RNA were seeded as 1.5×10^4 cells/well in a 96-well plate. The cells were immediately treated with various concentrations of remdesivir. The cells were also treated with 0.2% DMSO as a negative control because 10-µM remdesivir contains 0.2% DMSO. At 24 h post-treatment, the luminescence signal was detected as described above. Cell viability was measured by WST-1 assay following manufacture's protocol (Roche). The IC_{50} and CC_{50} were calculated using a four-parameter logistic regression model from the GraphPad Prism 5 software (GraphPad Software Inc.).

Data availability

All data generated or analyzed during this study are included in this published article (and its Supplementary Information file).

Received: 29 August 2020; Accepted: 14 January 2021
Published online: 26 January 2021

References

1. Guan, W. J. *et al.* Clinical characteristics of coronavirus disease 2019 in China. *N. Engl. J. Med.* **382**, 1708–1720. https://doi.org/10.1056/NEJMoa2002032 (2020).
2. Wang, Y. *et al.* Remdesivir in adults with severe COVID-19: A randomised, double-blind, placebo-controlled, multicentre trial. *Lancet* **395**, 1569–1578. https://doi.org/10.1016/S0140-6736(20)31022-9 (2020).
3. Ge, F., Luo, Y., Liew, P. X. & Hung, E. Derivation of a novel SARS-coronavirus replicon cell line and its application for anti-SARS drug screening. *Virology* **360**, 150–158. https://doi.org/10.1016/j.virol.2006.10.016 (2007).
4. Wang, J. M., Wang, L. F. & Shi, Z. L. Construction of a non-infectious SARS coronavirus replicon for application in drug screening and analysis of viral protein function. *Biochem. Biophys. Res. Commun.* **374**, 138–142. https://doi.org/10.1016/j.bbrc.2008.06.129 (2008).
5. Hartenian, E. *et al.* The molecular virology of coronaviruses. *J. Biol. Chem.* https://doi.org/10.1074/jbc.REV120.013930 (2020).
6. Yount, B. *et al.* Reverse genetics with a full-length infectious cDNA of severe acute respiratory syndrome coronavirus. *Proc. Natl. Acad. Sci. U.S.A.* **100**, 12995–13000. https://doi.org/10.1073/pnas.1735582100 (2003).
7. Almazán, F. *et al.* Construction of a severe acute respiratory syndrome coronavirus infectious cDNA clone and a replicon to study coronavirus RNA synthesis. *J. Virol.* **80**, 10900–10906. https://doi.org/10.1128/JVI.00385-06 (2006).
8. Scobey, T. *et al.* Reverse genetics with a full-length infectious cDNA of the Middle East respiratory syndrome coronavirus. *Proc. Natl Acad. Sci. U.S.A.* **110**, 16157–16162. https://doi.org/10.1073/pnas.1311542110 (2013).
9. Xie, X. *et al.* An infectious cDNA clone of SARS-CoV-2. *Cell Host Microbe* **27**, 841–848. https://doi.org/10.1016/j.chom.2020.04.004 (2020).

10. Thi, N. *et al.* Rapid reconstruction of SARS-CoV-2 using a synthetic genomics platform. *Nature* **582**, 561–565. https://doi.org/10.1038/s41586-020-2294-9 (2020).
11. Hou, Y. J. *et al.* SARS-CoV-2 reverse genetics reveals a variable infection gradient in the respiratory tract. *Cell* **182**, 429-446.e14. https://doi.org/10.1016/j.cell.2020.05.042 (2020).
12. Ye, C. *et al.* Rescue of SARS-CoV-2 from a single bacterial artificial chromosome. *mBio* **11**, e02168. https://doi.org/10.1128/mBio.02168-20 (2020).
13. Torii, S. *et al.* Establishment of a reverse genetics system for SARS-CoV-2 using circular polymerase extension reaction. *bioRvix* https://doi.org/10.1101/2020.09.23.309849 (2020).
14. Samavarchi-Tehrani, P. *et al.* A SARS-CoV-2—host proximity interactome. *bioRxiv* https://doi.org/10.1101/2020.09.03.282103 (2020).
15. Kumar, P. *et al.* The nonstructural protein 8 (nsp8) of the SARS coronavirus interacts with its ORF6 accessory protein. *Virology* **366**, 293–303. https://doi.org/10.1016/j.virol.2007.04.029 (2007).
16. Wang, M. *et al.* Remdesivir and chloroquine effectively inhibit the recently emerged novel coronavirus (2019-nCoV) in vitro. *Cell Res.* **30**, 269–271. https://doi.org/10.1038/s41422-020-0282-0 (2020).
17. Xie, X. *et al.* A nanoluciferase SARS-CoV-2 for rapid neutralization testing and screening of anti-infective drugs for COVID-19. *Nat. Commun.* **11**, 5214. https://doi.org/10.1038/s41467-020-19055-7 (2020).
18. Xia, H. *et al.* Evasion of type I interferon by SARS-CoV-2. *Cell Rep.* **33**, 108234. https://doi.org/10.1016/j.celrep.2020.108234 (2020).
19. Zhang, Y. *et al.* A bacterial artificial chromosome (BAC)-vectored noninfectious replicon of SARS-CoV-2. *Antiviral Res.* **185**, 104974. https://doi.org/10.1016/j.antiviral.2020.104974 (2020).
20. Otsuki, K. *et al.* Studies on avian infectious bronchitis virus (IBV). III. Interferon induction by and sensitivity to interferon of IBV. *Arch. Virol.* **60**, 249–255. https://doi.org/10.1007/BF01317496 (1979).
21. Hiscox, J. A., Cavanagh, D. & Britton, P. Quantification of individual subgenomic mRNA species during replication of the coronavirus transmissible gastroenteritis virus. *Virus Res.* **36**, 119–130. https://doi.org/10.1016/0168-1702(94)00108-o (1995).
22. Tamura, T. *et al.* In vivo dynamics of reporter Flaviviridae viruses. *J. Virol.* **93**, e01191-e1219. https://doi.org/10.1128/JVI.01191-19 (2019).
23. Schelle, B. *et al.* Selective replication of coronavirus genomes that express nucleocapsid protein. *J. Virol.* **79**, 6620–6630. https://doi.org/10.1128/JVI.79.11.6620-6630.2005 (2005).
24. Grossoehme, N. E. *et al.* Coronavirus N protein N-terminal domain (NTD) specifically binds the transcriptional regulatory sequence (TRS) and melts TRS-cTRS RNA duplexes. *J. Mol. Biol.* **394**, 544–557. https://doi.org/10.1016/j.jmb.2009.09.040 (2009).
25. Chang, C. K. *et al.* Modular organization of SARS coronavirus nucleocapsid protein. *J. Biomed. Sci.* **13**, 59–72. https://doi.org/10.1007/s11373-005-9035-9 (2006).
26. Pachetti, M. *et al.* Emerging SARS-CoV-2 mutation hot spots include a novel RNA-dependent-RNA polymerase variant. *J. Transl. Med.* **18**, 179. https://doi.org/10.1186/s12967-020-02344-6 (2020).
27. Toyoshima, Y. *et al.* SARS-CoV-2 genomic variations associated with mortality rate of COVID-19. *J. Hum. Genet.* **65**, 1–8. https://doi.org/10.1038/s10038-020-0808-9 (2020).
28. Ozono, S. *et al.* Naturally mutated spike proteins of SARS-CoV-2 variants show differential levels of cell entry. *bioRxiv* https://doi.org/10.1101/2020.06.15.151779 (2020).
29. Centers for Disease Control and Prevention (CDC). Research Use Only 2019-Novel Coronavirus (2019-nCoV) Real-time RT-PCR Primers and Probes. https://www.cdc.gov/coronavirus/2019-ncov/lab/rt-pcr-panel-primer-probes.html
30. Schindelin, J. *et al.* Fiji: an open-source platform for biological-image analysis. *Nat. Methods* **9**, 676–682. https://doi.org/10.1038/nmeth.2019 (2012).

Acknowledgements

This work was supported by a young scientist dispatch program, Kobe University: by a subsidy for post-corona society realization, Hyogo prefecture, and by Japan Agency for Medical Research and Development (AMED) under Grant Number JP20he082206. The manuscript was proofread by Enago. We thank Ms. Honoka Yoneda for her technical assistance. We also thank Dr. Masayuki Saijo of the National Institute of Infectious Diseases for providing RNA of SARS-CoV-2 JPN AI/I 004 strain.

Author contributions

T.K. and M.K. conceived the study. T.K. performed the experiments and took the lead in writing the manuscript. X.X., P.Y.-S., and M.K. provided feedback and helped shape the research and manuscript.

Competing interests

The authors declare no competing interests.

Additional information

Supplementary Information The online version contains supplementary material available at https://doi.org/10.1038/s41598-021-82055-0.

Correspondence and requests for materials should be addressed to T.K. or M.K.

Reprints and permissions information is available at www.nature.com/reprints.

Publisher's note Springer Nature remains neutral with regard to jurisdictional claims in published maps and institutional affiliations.